Available online at www.sciencedirect.com
ScienceDirect
Journal of Solid State Chemistry 180 (2007) 2661–2669
JOURNAL OF SOLID STATE CHEMISTRY
www.elsevier.com/locate/jssc

Synthesis of nano-sized crystalline oxide ion conducting fluorite-type Y_2O_3-doped CeO_2 using perovskite-like $BaCe_{0.9}Y_{0.1}O_{2.95}$ (BCY) and study of CO_2 capture properties of BCY

B.R. Sneha, V. Thangadurai*

Department of Chemistry, University of Calgary, 2500 University Drive NW, Calgary, Alberta, Canada T2N 1N4

Received 5 June 2007; received in revised form 19 July 2007; accepted 24 July 2007
Available online 7 August 2007

Abstract

Formation of nano-sized Y_2O_3-doped CeO_2 (YCO) was observed in the chemical reaction between proton conducting Y_2O_3-doped $BaCeO_3$ (BCY) and CO_2 in the temperature range 700–1000 °C, which is generally prepared by wet-chemical methods that include sol–gel, hydrothermal, polymerization, combustion, and precipitation reactions. BCY can capture CO_2 of 0.13 g per ceramic gram at 700 °C, which is comparable to that of the well-known Li_2ZrO_3 (0.15 g per ceramic gram at 600 °C). Powder X-ray diffraction (PXRD), energy dispersive X-ray analysis (EDX), laser particle size analysis (LPSA), scanning electron microscopy (SEM), transmission electron microscopy (TEM), and ac impedance spectroscopy were employed to characterize the reaction product obtained from reaction between BCY and CO_2 and subsequent acid washing. PXRD study reveals presence of fluorite-like CeO_2 ($a = 5.410$ (1) Å) structure and $BaCO_3$ in reaction products. TEM investigation of the acid washed product showed the formation of nano-sized material with particle sizes of about 50 nm. The electrical conductivity of acid washed product (YCO) in air was found to be about an order higher than the undoped CeO_2 reported in the literature.

Keywords: Nano-materials; Y_2O_3-doped CeO_2 (YCO); Y_2O_3-doped $BaCeO_3$ (BCY); CO_2 capturing; Oxide ion electrolyte; Transmission electron microscopy (TEM); AC impedance

1. Introduction

Ionic devices that utilize solid-state proton conductors (SSPCs) play important role in the generation and storage of alternative energy, electrolysis, H_2 storage, H_2 separation, electrochromics, gas sensors as well as maintenance of natural environment [1–10]. SSPCs based on a perovskite-like ABO_3 (A = Ca, Sr, Ba; B = Ti, Zr, Ce) structure are being considered as a promising solid electrolyte to replace the current solid oxide fuel cells (SOFCs) electrolyte Y_2O_3-doped ZrO_2 (YSZ), due to their high ionic (H^+) conduction. Among them, Y_2O_3-doped $BaCeO_3$ (BCY) is one of the well-known and investigated in detail to understand the chemical composition–structure–electrical transport property relationship [2,11–17]. The origin of proton conduction in BCY has been investigated intensively by many authors, and confirmed that the conduction occurs by means of the defect equilibrium reactions between the oxygen vacancies ($V_O^{\bullet\bullet}$), holes ($h^{\bullet}$), lattice oxygen (O_O^x)and water vapour at elevated temperatures [1–22]. Using Kröger–Vink notation [23], it can be written as

$$H_2O_{(g)} + V_O^{\bullet\bullet} + O_O^x \rightarrow 2OH_O^{\bullet}, \quad (1)$$

where $OH_O^{\bullet}$ represents a proton attached to the lattice oxygen. The proton conduction in BCY occurs via a Grotthuss (hopping) mechanism between adjacent BO_6 octahedra [2].

Although, BCY has been demonstrated as a potential solid electrolyte for applications to various ionic devices, it is not practically suitable for commercialization. This is as a result of its chemical and structural instability in humidity (a common by-product in fuel cells that utilize hydrogen and hydrocarbons as fuels), and CO_2 atmospheres (present

*Corresponding author. Fax: +1 403 289 9488.
E-mail address: vthangad@ucalgary.ca (V. Thangadurai).

0022-4596/$ - see front matter © 2007 Elsevier Inc. All rights reserved.
doi:10.1016/j.jssc.2007.07.016

commonly in the hydrocarbon fuels) at elevated temperatures. Several researchers have reported the formation of $Ba(OH)_2$ and $BaCO_3$ in water and CO_2, respectively [9,24–35]. Partial or complete substitutions of tetravalent Zr^{4+} ions for Ce^{4+}, and Sr^{2+} or Ca^{2+} ions for Ba^{2+} in BCY have found to improve the chemical stability of BCY in CO_2 [27]. However, the substitution of Zr^{4+} for Ce^{4+} in BCY found to decrease the proton conductivity than that of BCY, as well as exhibited a poor mechanical stability [27–31]. For example, H_2 permeation through Ni–Zr-doped BCY was found to degrade rapidly about 53% within 4 h and ~72–91% after 2–7 h of exposure to 30% CO_2 at 900 °C [32]. Thus, there is a lack of fast SSPCs with high chemical stability against CO_2 and water, and proton conductivity to replace the YSZ in SOFCs development.

The primary aim of the present work is to (i) investigation on a long-term structural stability of BCY in 100% CO_2 in the temperature range 600–1000 °C, compare its CO_2 capturing ability with other well-known metal oxides, and (ii) examine the by-product obtained after reaction with CO_2 and subsequent acid washing employing various solid-state characterization methods that include powder X-ray diffraction (PXRD), laser particle size analyser (LPSA), scanning electron microscopy (SEM), transmission electron microscopy (TEM) and ac impedance spectroscopy. The former study shows that BCY could be considered a potential CO_2 capturing agent (0.13 g per ceramic gram at 700 °C), but, its theoretical capacity is only 0.14 g per ceramic gram. Very interestingly, the latter study confirmed the formation of nano-sized crystals of Y_2O_3-doped CeO_2 (YCO), and is a different route from the already well-known soft-chemical methods such as sol–gel, polymerization, hydrothermal, precipitations, and combustion techniques.

2. Experimental

2.1. Preparation and phase characterization

$BaCe_{0.9}Y_{0.1}O_{2.95}$ (BCY) was prepared by a conventional solid-state reaction in air using appropriate amounts of $BaCO_3$ (>99.8% Fisher Scientific Co.), CeO_2 (>99.9% Alfa Aesar) and Y_2O_3 (>99.9% Alfa Aesar) at elevated temperature of 1450 °C for 24 h (Carbolite RHF16/3, England). The reactant powders were mixed in a ball mill (Pulverisette, Fritsch, Germany) using zirconia balls in 2-propanol at 200 rpm for 6 h with intermediate change in the rotation direction each hour, to avoid improper mixing. The mixed powders were first heated at 800 °C for 12 h and then at 1450 °C for 24 h in air, with a heating and cooling rate of 10 °C per min, with repeated mixing procedures at each step. In the final stage of heat treatment, the reaction products were pressed into pellets by isostatic pressure. The sintered pellets were crushed into powders for phase characterization employing PXRD (Cu$K\alpha$) (Rigaku Powder X-ray Diffractometer (Cu$K\alpha$), Japan) at room temperature (RT). The lattice constant was determined from powder XRD data by least-squares refinement.

A known quantity (about 20 g) of BCY powder was reacted in flowing 100% CO_2 at the temperature range 600–1000 °C for 48 h. After the reaction, the sample was cooled to RT under passing CO_2. The weight gain in the sample was measured using an analytical balance. Then, the powders were washed with dilute HCl. Acid was added until all the CO_2 evolved and the sample was filtered and dried in ambient atmosphere at RT. The resultant powder sample was characterized using PXRD, SEM, and energy dispersive X-ray analysis (Philips XL30 SEM, The Netherlands) and TEM (Hitachi H700, TEM, Japan). The particle size distribution of powders was determined using a LPSA (NanoTec Analysette 22, Fritsch, Germany). The powder was dispersed homogeneously in water using ultrasound for determination of particle sizes.

2.2. Electrical conductivity measurements

Electrical conductivity measurements of pellets (~0.15 cm in thickness and ~1 cm in diameter) of the acid washed powder (sintered at 1400 °C for 24 h in ambient atmosphere) was performed in air using Pt-electrodes (Pt-paste obtained from Heraeus Inc., LP A88-11S, Germany, cured at 850 °C in air for 1 h to remove the organic binders) and employing AC impedance and gain-phase analyser (SI model no. 1260) (0.1 Hz–15 MHz). A two probe electrochemical cell was used. The applied ac voltage was 10 mV. Before each electrical measurement, the sample was equilibrated at constant temperature for 2–8 h. The measurements were made for two subsequent heating and cooling runs.

3. Results and discussion

3.1. Chemical stability of BCY in CO_2 and its CO_2 capturing capacity

PXRD study of BCY confirms the formation of single-phase perovskite-like structure (Fig. 1a). We could index an orthorhombic cell with lattice parameters of $a = 8.697(5)$ Å, $b = 6.107$ (5) Å and $c = 6.266$ (3) Å which is comparable to those of the literature data (for e.g., $a = 8.75847(4)$ Å; $b = 6.22666(3)$ Å; $c = 6.21109(3)$ Å) [11] and ($a = 8.764(1)$ Å; $b = 6.233(1)$ Å; $c = 6.211(1)$ Å) [12]. BCY powders heated in CO_2 in the temperature range 700–1000 °C show a complex diffraction pattern, and is due to $BaCO_3$ and fluorite-like structure CeO_2 (Fig. 1b). Also, we do not see the characteristic diffraction peaks (100–40% intensity) attributable to the formation of Y_2O_3 in the decomposition products obtained over the investigated temperature range (600–1000 °C). Our result corroborates with the literature report that BCY is chemically stable in CO_2 at 600 °C [24–35]. The acid washed product shows the formation of the fluorite-type CeO_2 pattern (Fig. 1d) while the sample reheated in air at 1400 °C shows the original

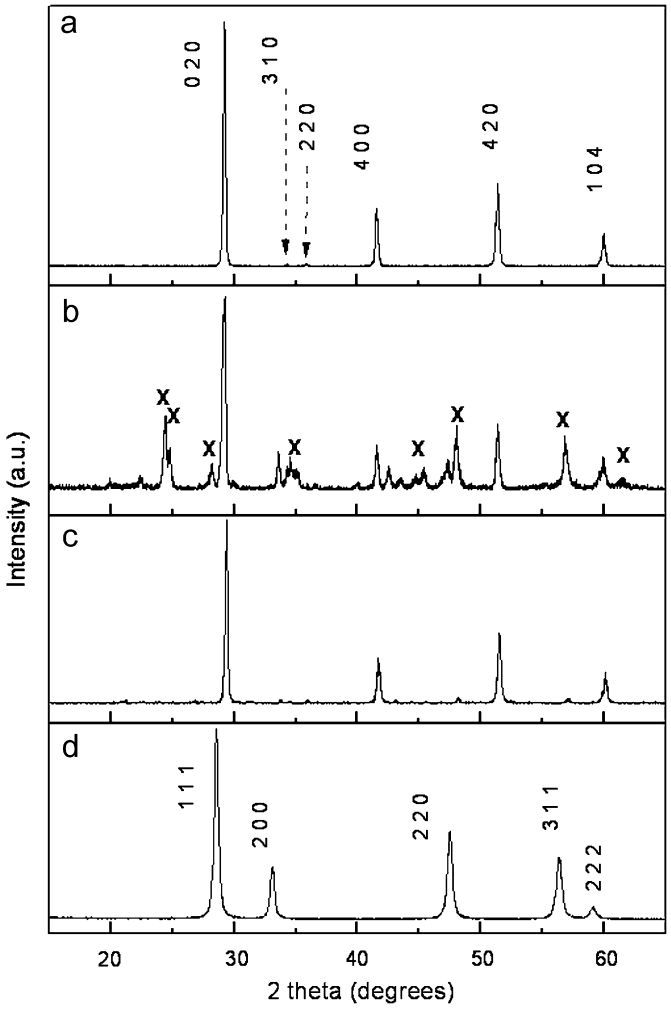

Fig. 1. Powder XRD patterns showing the reactivity of $BaCe_{0.9}Y_{0.1}O_{2.95}$ (BCY) with CO_2 at 700 °C for 48 h: (a) as prepared BCY—shows the formation of ABO_3 perovskite structure ($a = 8.697(5)$ Å; $b = 6.107$ (5) Å; $c = 6.266(3)$ Å) and consistent with literature; (b) BCY reacted with CO_2 at 700 °C—shows the sample 'a' decomposed into $BaCO_3$ + reaction products; (c) sample 'b' reheated in air at 1400 °C for 24 h-shows the formation of the sample 'a' and (d) sample 'b' washed with dilute HCl and dried in ambient atmosphere—confirms the formation of fluorite-like CeO_2 structure ($a = 5.410$ (1) Å).

perovskite-like structure (Fig. 1c). The following chemical reaction can be proposed to explain decomposition:

$$BaCe_{0.9}Y_{0.1}O_{3-\delta}(BCY)_{(s)} + CO_{2(g)} \overset{700-1000\,^{\circ}C}{\underset{1400\,^{\circ}C,\ \text{in air}}{\rightleftharpoons}} BaCO_{3(s)} + Ce_{0.9}Y_{0.1}O_{1.95(s)} \overset{\text{aq.HCl}}{\longrightarrow} Ce_{0.9}Y_{0.1}O_{1.95(s)} + CO_{2(g)} \uparrow + Ba(OH)_{2(aq)}. \quad (2)$$

This first step in reaction (2) indicates that BCY can be explored as a potential CO_2 capturing agent in the temperature range 700–1000 °C. At 700 °C, we found that BCY can absorb 0.13 g of CO_2 per ceramic gram. The theoretical CO_2 capture of BCY is 0.14 g per ceramic gram of BCY, while other metal oxides, including Li_2O and Li_2SiO_4 exhibit much higher theoretical capacity [36–46]. In Table 1, we compare the CO_2 capturing property of BCY with other well-known metal oxides. It is very interesting to note that BCY (at 700 °C) absorbs nearly the same amount of CO_2 to that of Li_2ZrO_3 (0.15 g per gram at 600 °C) which is about 48–57% lower than those of Li_4SiO_4 [37], $Li_6Zr_2O_7$ [41], and Na_2ZrO_3 [39]. This is due to high molecular weight of BCY and hence, BCY appears not to be an efficient material for CO_2 capture application. At temperature below 600 °C, BCY does not capture CO_2 because it is kinetically not favourable to from $BaCO_3$ [30]. The CO_2 absorption property of Li_2ZrO_3 and CaO are efficient only below 700 °C, and increasing temperature further the desorption of CO_2 occurs, as confirmed by thermodynamic calculations [37,46]. Therefore, these materials are not suitable for CO_2 capture at elevated temperatures (> 700 °C) while BCY could be considered as a potential alternative for high-temperature applications.

All the diffraction peaks of the acid washed and 1400 °C heated sample were found to be shifted to lower two theta compared with the undoped CeO_2 ($a = 5.403$ (1) Å for commercially available powders from Alfa Aesar). We could index the PXRD of acid washed product heated at 1400 °C on cubic fluorite-type lattice constant with $a = 5.379(3)$ Å and is consistent with literature [47,48]. Based on the ionic radii consideration, one would expect that Y-doped CeO_2 should show higher lattice constant than undoped CeO_2. The ionic radius for Ce^{4+} ion at the eight fold is 0.97 Å and the corresponding value for Y^{3+} is 1.015 Å [49]. But, the opposite effect was explained in the literature by considering oxide ion vacancy formation [47,48]. Hence, the acid washed product would be called as YCO here after.

The fluorite structure (AO_2) consists of cubic close packed array of A^{4+} cations (surrounded by eight oxygen ions) and O^{2-} ions occupy the tetrahedral (surrounded by four A-cations) sites [50]. The ideal perovskite ($SrTiO_3 \equiv ABO_3$) exhibits a primitive cubic structure that consists of cubic close packing of 'A + 3O' unit and B cations are distributed at the octahedral interstitial site [51]. The A cations occupy the centre of cube at the 12-fold coordination site. Depending on the A- and B-site cations, tetragonal, orthorhombic and monoclinic structure perovskites were reported [51]. In BCY, the large size Ba^{2+} ions occupy the A-site and Ce^{4+} and Y^{3+} ions occupy the B-site [11]. Virkar et al. proposed metal oxygen bond breaking and a diffusive transport of ions to allow the conversion of BCY into YCO and $BaCO_3$ in CO_2 [25,26]. Fig. 2 shows the schematic representation of the conversion of perovskite-like BCY into fluorite-like structure YCO and $BaCO_3$ in CO_2 at 700–1000 °C. The electrical conductivity studies reported high mobility for oxide ions and protons in H-atom containing atmospheres in BCY [1–22], while the A- and B-site cations mobility are not known at present. A detailed in-situ XRD investigation in combination with chemical analysis under CO_2 at elevated temperature may be useful to elucidate the actual mechanism for the proposed degradation reaction Eq. (2).

Table 1
Comparison of potential CO_2 capturing metal oxides and their theoretical and experimental CO_2 absorbing values with $BaCe_{0.9}Y_{0.1}O_{2.95}$ (BCY)

Materials	Theoretical CO_2 capturing per ceramic gram	Experimentally observed CO_2 capturing per ceramic gram	Temperature (°C)	References
Li_2O	1.46	1.26	600	[39]
MgO	1.09	1.09	600	[38]
CaO	0.78	0.73	600	[40,45]
Li_2ZrO_3	0.28	0.15	600	[39,43,44]
$Li_6Zr_2O_7$	0.39	0.25	600	[41]
Li_4SiO_4	0.73	0.30	600	[38,39]
Na_2ZrO_3	0.24	0.25	600	[39,42]
$Sr_{0.95}Ca_{0.05}Fe_{0.5}Co_{0.5}O_{3-\delta}$	0.3	0.17	820	[36]
BCY	0.14	Negligible	600	Present work
BCY	0.14	0.13	700	Present work
BCY	0.14	0.103	1000	Present work

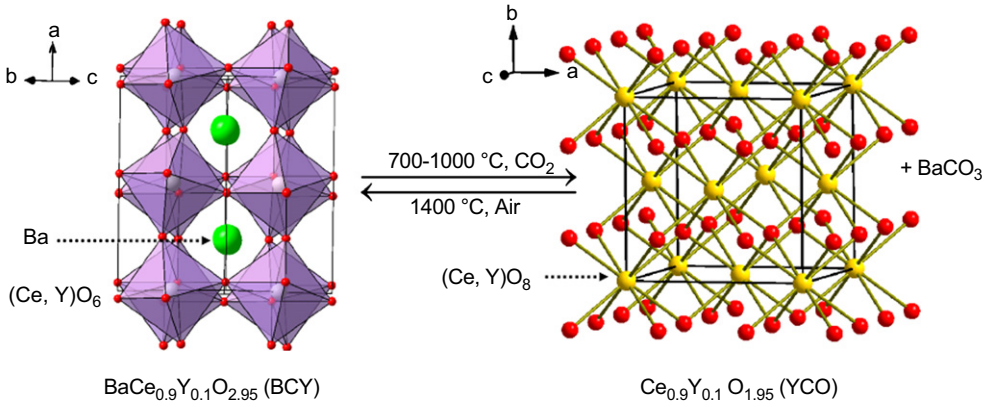

Fig. 2. Idealized crystal structure showing the conversion of the perovskite-like structure $BaCe_{0.9}Y_{0.1}O_{2.95}$ (BCY) into a fluorite-like Y_2O_3-doped CeO_2 (YCO) and $BaCO_3$ in CO_2 at 700 °C.

3.2. Microstructure characterization of YCO

Typical SEM and TEM images of YCO prepared from BCY are shown in Figs. 3 and 4, respectively. As prepared acid washed YCO exhibits irregular size distribution of large agglomerates (Fig. 3a) and the sintered sample shows a homogeneous distribution of particles (Fig. 3b). The elemental analysis confirmed the absence of Ba^{2+} ions and presence of Ce^{4+} and Y^{3+} ions in the acid washed product, which is consistent with the diffraction study (Fig. 1d). TEM study clearly indicates the presence of nano-sized YCO particles of less than 50 nm in both acid washed product (Fig. 4a) and subsequently heated YCO powder at 1400 °C for 24 h (Fig. 4b).

In Fig. 5, we show the particle size distribution of acid washed YCO (Fig. 5a) and the powder sample heated at 1400 °C in air for 24 h (Fig. 5b) obtained using LPSA. We see both samples exhibit similar particle size distributions except aggregates of about 50–90 μm was observed in the sintered sample and is attributed to sintering. Very interestingly, we observe that both techniques show the presence of nano-sized particles. A similar correlation study was performed for the lithium lanthanum titanates [52]. It must be mentioned that several wet chemical methods that include hydrothermal [53], precipitation [54–57], combustion [58], polymerization [59], template [60], and sol–gel [61] were developed recently to prepare the nano-sized particles of ceria. The present method utilizes conventional solid-state synthesized BCY as starting material to prepare YCO. We believe this method can be extended to prepare several other doped CeO_2 with nano-sized particles.

Fig. 6 shows the TEM images of the sintered pellet crushed into powders after electrical measurements in air up to 800 °C. We see much higher particle sizes (ca. 200–500 nm) compared to that of as-prepared powder sample (Fig. 4a), confirming the particles growth due to sintering. This was further confirmed by the LPSA measurements (Fig. 5). We have also observed large aggregates of particles in the range of 10–100 μm in the 1400 °C sintered YCO sample (Fig. 5b) together with nano-particles. Stabilization of nano-sized particles at elevated temperatures over a long period of time is a common issue in the high-temperature materials applications that include SOFCs, catalysis, as well as solid-state gas sensors.

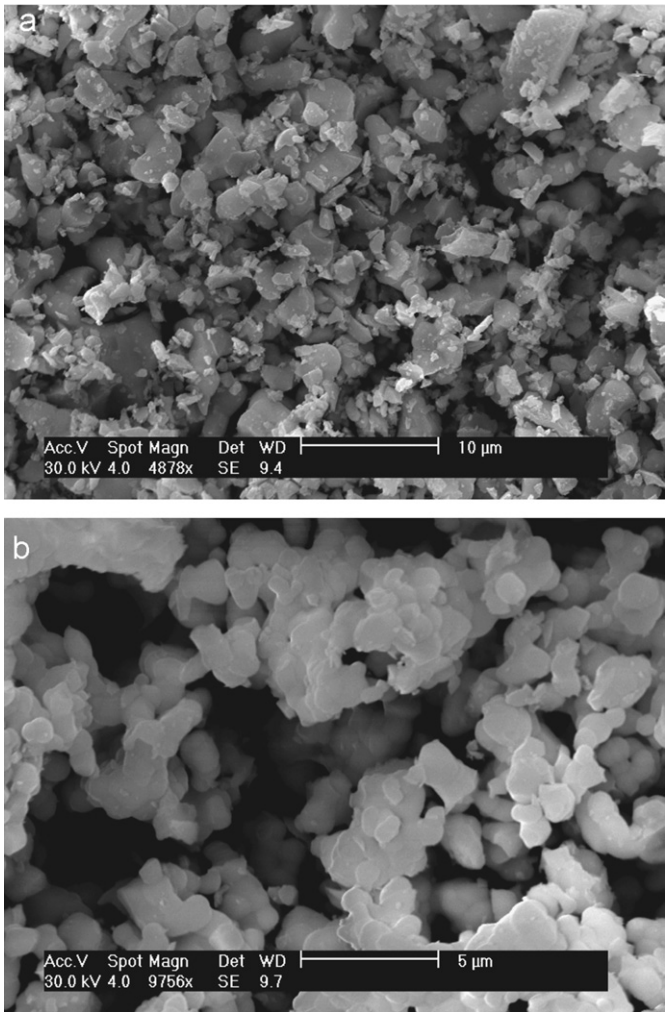

Fig. 3. Scanning electron microscope (SEM) images of the fluorite-type powders (a) obtained by acid washing of the reaction product (Fig. 1d), (b) sample 'a' heated at 1400 °C for 24 h in air.

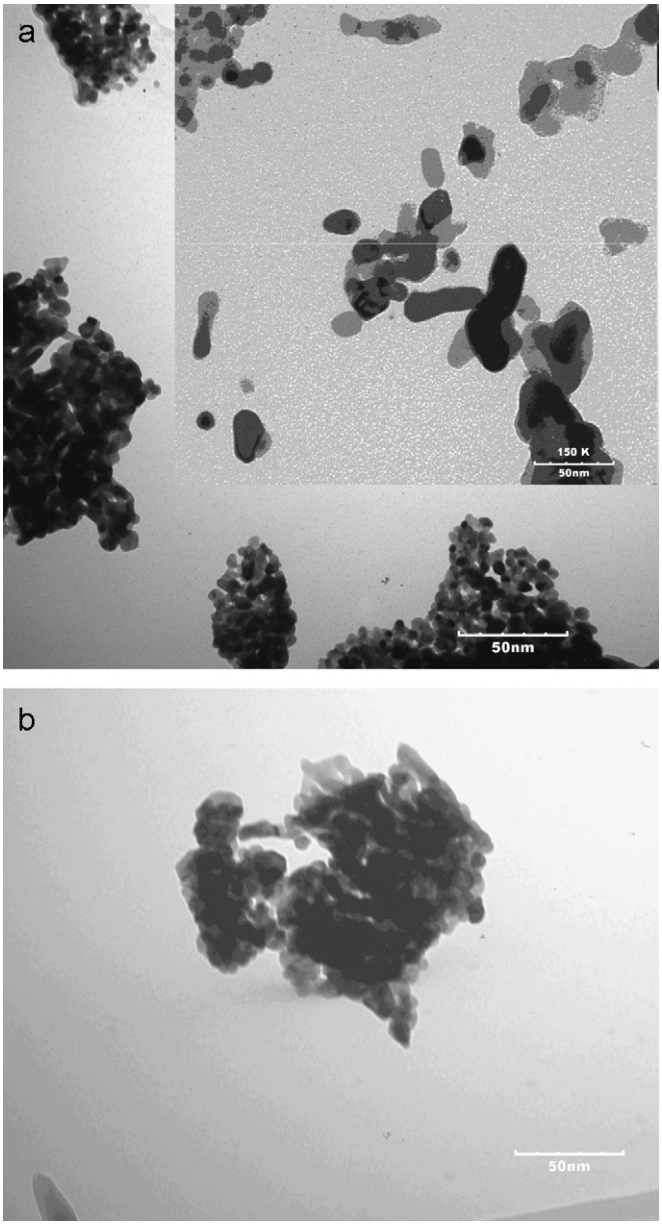

Fig. 4. Transmission electron microscope (TEM) images of (a) the fluorite-type powders obtained by acid washing of the reaction product (Fig. 1d), (b) powder sample 'a' heated at 1400 °C in air for 24 h. The inset in Fig. 4a shows the presence of nano-particles in different region of the sample.

3.3. Electrical conductivity of nano-YCO

Fig. 7 shows the typical AC impedance plots of YCO (acid washed product) at 320, 430, and 825 °C in air. Two distinct semicircles at the high frequency side and a 'tail' at low frequency side are observed at temperature below 450 °C, which may be attributed to bulk and grain-boundary resistances and electrode effects [62]. Similar impedance plots were reported for the parent and doped CeO_2 [53,63–66]. The estimated bulk and grain-boundary conductivity was found to be 3.2×10^{-5} and 1.12×10^{-5} S/cm, respectively, at 320 °C. It is significant to mention that unlike solid-state reaction products, the nano-CYO prepared in this work exhibit similar order of bulk and grain-boundary electrical conductivity. Table 2 lists bulk, grain-boundary and total (bulk + grain-boundary) conductivity of YCO in the temperature range 200–430 °C. However, we did not clearly see both bulk and grain-boundary contributions over the entire temperature range of measurement. Also, the grain boundary and electrode contributions vary drastically with increasing temperature, especially above 450 °C, it was very difficult to separate accurately bulk, grain boundary, and electrode contribution. At very high temperatures, we see mainly electrode polarization resistance and an inductive effect at the low- and high-frequency region, respectively (Fig. 7c). Thus, we have taken uniformly the bulk resistance from the high-frequency minimum/intercept along the Z'-axis of the impedance plots to calculate the electrical conductivity data.

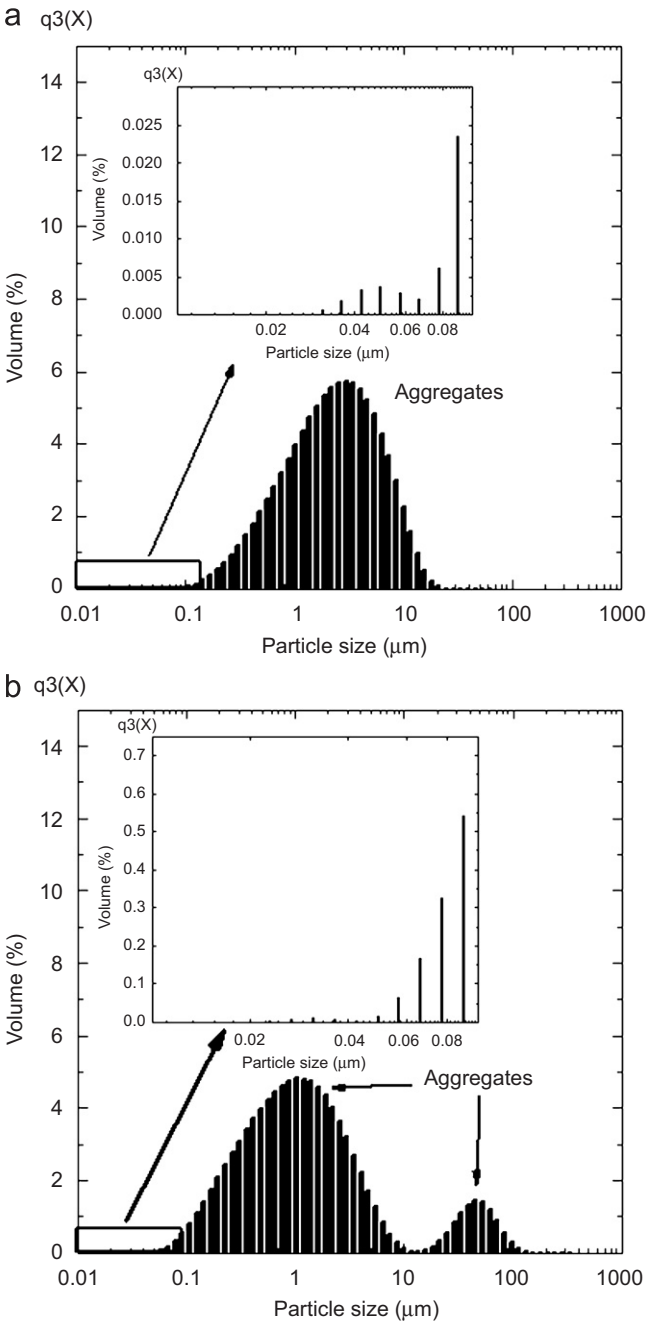

Fig. 5. Histogram of size of particles and aggregates distribution of (a) YCO-as prepared from the reaction of $BaCe_{0.9}Y_{0.1}O_{2.95}$ (BCY) with CO_2 and the acid washed product, and (b) powder sample 'a' heated at 1400 °C in air and ground using mortar and pestle.

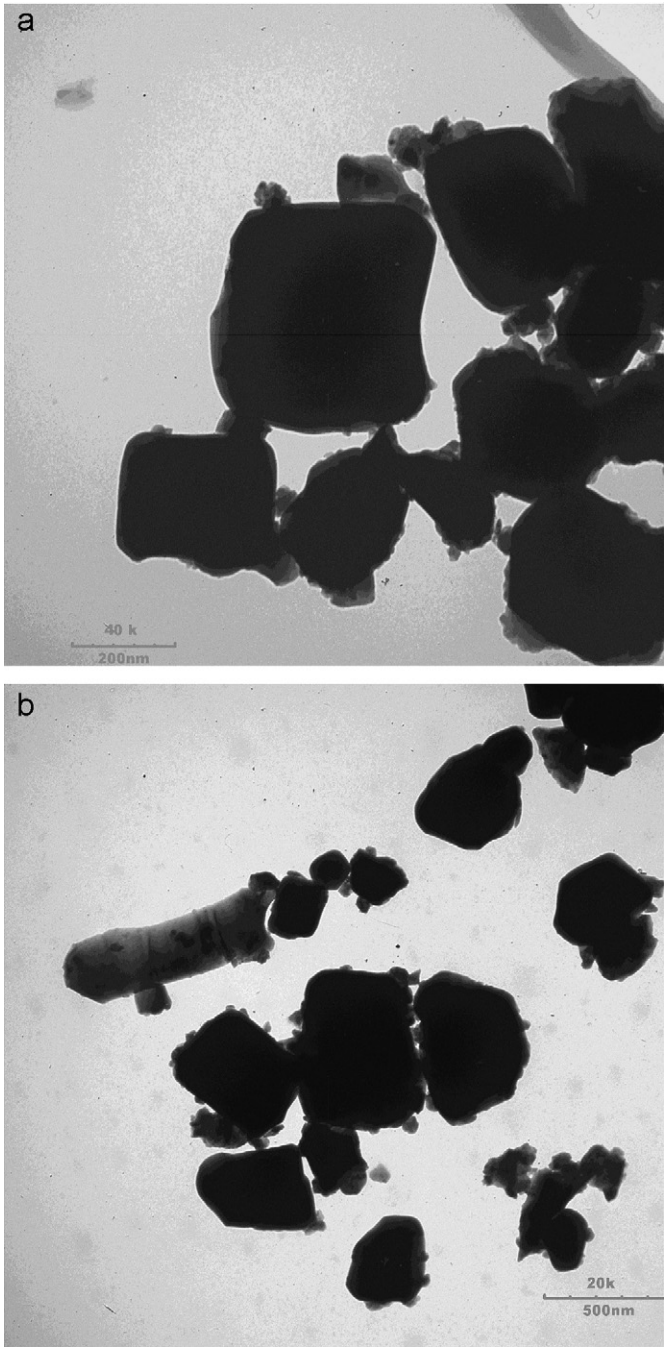

Fig. 6. Transmission electron microscope (TEM) images of YCO sample pellet after the electrical measurement, (a) and (b) show the typical growth of the particles in different regions of the sample due to sintering. The sample pellet was ground using mortar and pestle for the TEM study.

Fig. 8 shows the Arrhenius plot for the total (bulk + grain-boundary) ionic conductivity of YCO. The line passing through the data points is guide a to eye. The electrical conductivity data obtained during the first cycle heating and cooling and subsequent runs follow the same line, suggesting the equilibrium behaviour of the sample. The activation energy for total electrical conductivity was found to be 0.87 eV (for the second heating cycle), which is comparable to those of the literature values [53,63–73].

In Fig. 9, we compare the total electrical conductivity data of YCO with literature value of un-doped and acceptor doped CeO_2. Compared with pure CeO_2, we see clearly a significant increase in the electrical conductivity over the investigated temperature, and also is comparable to other acceptor doped CeO_2. This result supports that the

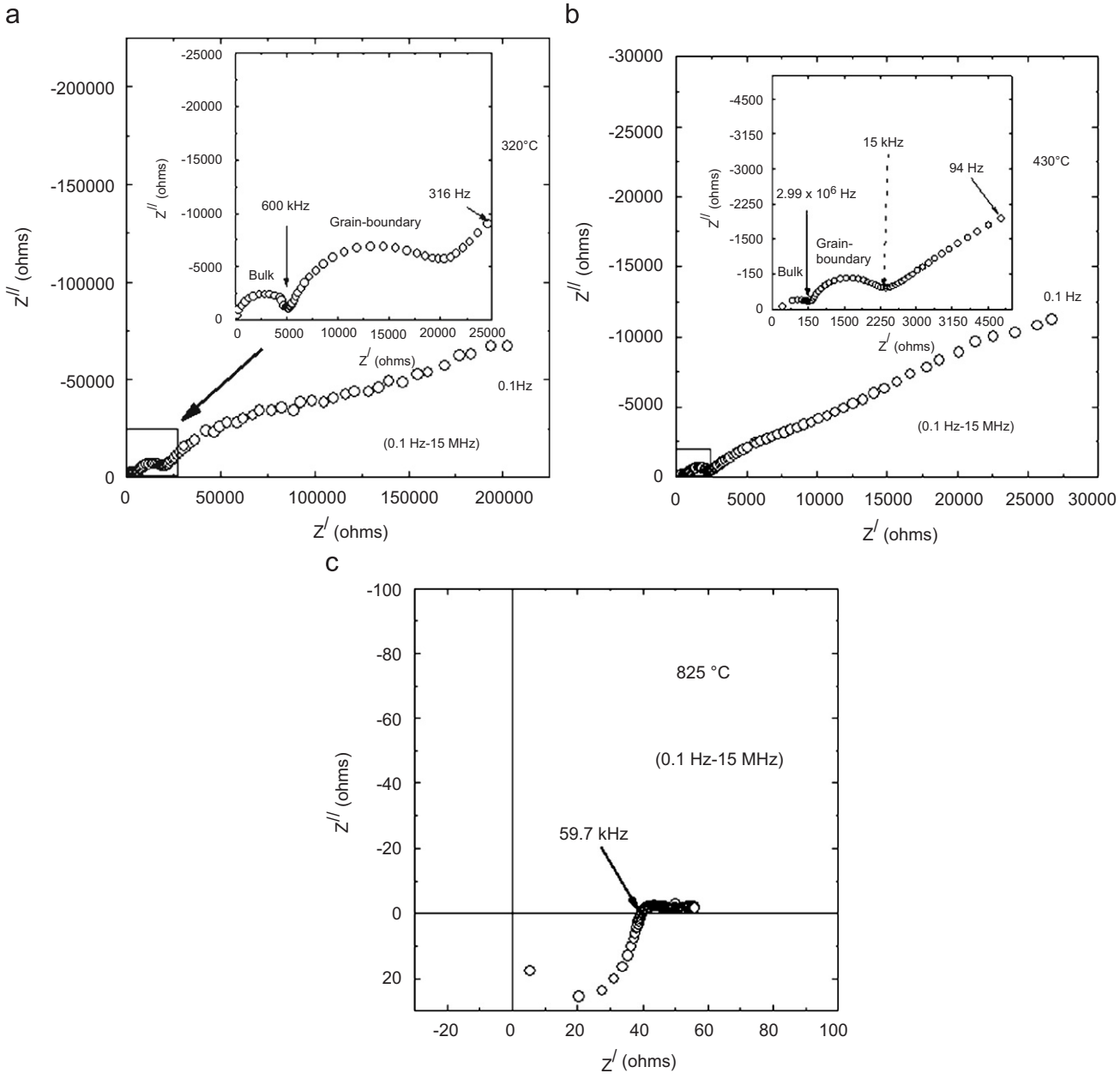

Fig. 7. AC impedance plots of Y_2O_3-doped CeO_2 (YCO) obtained from $BaCe_{0.9}Y_{0.1}O_{2.95}$ (BCY) in air at 320, 430 and 825 °C in the frequency range 0.1 Hz–15 MHz. The high frequency semicircle corresponds to bulk, intermediate frequency semicircle attributes to the grain-boundary resistance, and low-frequency part of impedance is due to electrode effect. Positive value of the imaginary component at high-temperature data shows the presence of inductive effect.

Table 2
Bulk, grain-boundary and total electrical conductivity of YCO prepared from BCY

Temperature (°C)	σ_{bulk} (S/cm)	$\sigma_{grain\text{-}boundary}$ (S/cm)	σ_{total} (S/cm)
207	8.43×10^{-7}	2.06×10^{-7}	1.65×10^{-7}
274	7.46×10^{-6}	1.62×10^{-6}	1.30×10^{-6}
320	3.20×10^{-5}	1.12×10^{-5}	7.35×10^{-6}
350	5.43×10^{-5}	1.75×10^{-5}	1.32×10^{-5}
376	9.20×10^{-5}	3.41×10^{-5}	2.54×10^{-6}
431	2.20×10^{-4}	1.05×10^{-4}	7.11×10^{-5}

Y^{3+} ion is doped in CeO_2, as proposed in BCY decomposition reaction (2) and also is consistent with PXRD data. Very interestingly, we see that our electrical conductivity data is comparable to some of the doped CeO_2 reported in the literature. However, there is a little difference between the present value and reported value for compounds at high temperature. It must be noted that electrical conductivity of the ceria-based materials depends on the sintering temperature and purity of the starting materials [71–73]. The small difference may be attributed to low sintering temperature employed in the present study.

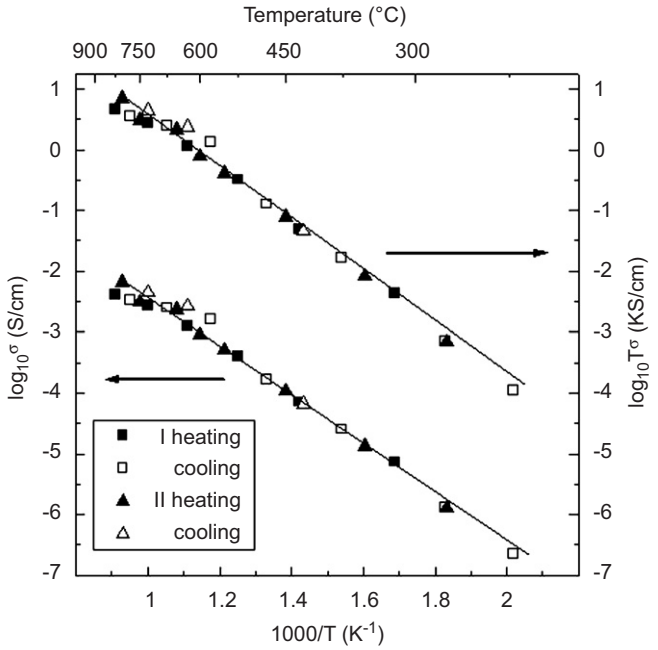

Fig. 8. Arrhenius plots for the total electrical conductivity data of Y_2O_3-doped CeO_2 (YCO) prepared from the reaction with $BaCe_{0.9}Y_{0.1}O_{2.95}$ (BCY). The line passing through the data points is a guide to the eye.

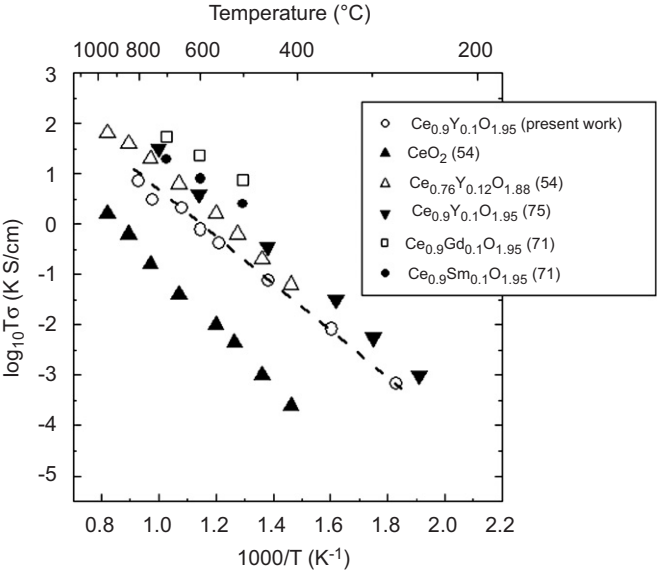

Fig. 9. Comparison of the total electrical conductivity data of Y_2O_3-doped CeO_2 (YCO) prepared by reaction between $BaCe_{0.9}Y_{0.1}O_{2.95}$ (BCY) and CO_2 literature data. We see the data obtained in this study is comparable to those reported for acceptor-doped CeO_2. The line passing through the data points is a guide to the eye.

4. Conclusions

In summary, we have shown that the reaction between BCY and 100% CO_2 in the temperature range 700–1000 °C gives a nano-sized crystalline YCO, which has been hitherto prepared commonly employing wet chemical methods. BCY can capture CO_2 above 700 °C (0.13 g per ceramic gram), however, it exhibits quite low theoretical capacity of 0.14 g per ceramic gram compared with other well-known compounds, for e.g., Li_2O (1.76 g per ceramic gram), Li_2ZrO_3 (0.28 g per ceramic gram) and CaO (0.78 g per ceramic gram). The experimental CO_2 capture of BCY was found to be about 93% (0.13 g per gram of BCY) at the investigated temperature which is higher than Li_2O (86%); Li_2ZrO_3 (54%) and comparable to CaO (95%). The PXRD investigation confirms that CeO_2 and Y_2O_3 were stable against chemical reaction with CO_2. SEM and TEM studies on the microstructure reveal the formation of nano-sized materials of YCO. The electrical conductivity on acid washed material (YCO) exhibits more than one order higher electrical conductivity than that of the undoped CeO_2. The activation energy and total conductivity of YCO were found to be comparable to the ceramic method prepared YCO samples with a similar chemical composition.

Acknowledgments

V. Thangadurai would like to thank the Natural Sciences and Engineering Research Council (NSERC) of Canada for funding through the Research and Tools Instrumentation (RTI) (cat. 1), and Discovery Grants (DG), and the University of Calgary for financial support through start-up grants. One of us (B.R. Sneha) thanks the Institute for Sustainable Energy, Environment and Economy (ISEEE) of the University of Calgary for ISEEE graduate scholarship.

References

[1] H. Iwahara, Solid State Ionics 52 (1992) 99–104.
[2] K.D. Kreuer, Chem. Mater. 8 (1996) 610–641.
[3] T. Norby, Solid State Ionics 125 (1999) 1–11.
[4] G. Alberti, M. Casciola, Solid State Ionics 145 (2001) 3–16.
[5] W. Grover Coors, J. Power Sources 118 (2003) 150–156.
[6] H. Iwahara, Solid State Ionics 125 (1999) 271–278.
[7] H. Iwahara, Y. Asakura, K. Katahira, M. Tanaka, Solid State Ionics 168 (2004) 299–310.
[8] H. Matsumoto, S. Okada, S. Hashimoto, K. Sasaki, R. Yamamoto, M. Enoki, T. Ishihara, Ionics 13 (2007) 93–99.
[9] J.W. Phair, S.P.S. Badwal, Ionics 12 (2006) 103–115.
[10] Ph. Colomban (Eds.), Solid State Proton Conductors Solids-Membranes and Gels-Materials and Devices, Cambridge University Press, Cambridge, 1992.
[11] K.S. Knight, Solid State Ionics 127 (2000) 43–48.
[12] K. Takeuchi, C.K. Loong, J.W. Richardson, J. Guan, S.E. Dorris, U. Balachandran, Solid State Ionics 138 (2000) 63–77.
[13] A. Kruth, R.A. Davies, M.S. Islam, J.T.S. Irvine, Chem. Mater. 19 (2007) 1239–1248.
[14] K.D. Kreuer, Solid State Ionics 97 (1997) 1–15.
[15] K.D. Kreuer, Solid State Ionics 125 (1999) 285–302.
[16] K.D. Kreuer, Annu. Rev. Mater. Res. 33 (2003) 333–359.
[17] M.S. Islam, R.A. Davies, J.D. Gale, Chem. Comm (2001) 661–662.
[18] K.D. Kreuer, E. Schonherr, J. Maier, Solid State Ionics 70/71 (1994) 278–284.
[19] S. Steinsvik, Y. Larring, T. Norby, Solid State Ionics 143 (2001) 103–116.
[20] M. Wideroe, W. Munch, Y. Larring, T. Norby, Solid State Ionics 154-155 (2002) 699–777.

[21] J. Wu, R.A. Davies, M.S. Islam, S.M. Haile, Chem. Mater. 17 (2005) 846–851.
[22] A.S. Patnaik, A.V. Virkar, J. Electrochem. Soc. 153 (2006) A1397–A1405.
[23] F. A. Kröger, The Chemistry of Imperfect Crystals-Imperfection Chemistry of Crystalline Solids, 2nd Edition:Vol. 2, North-Holland Amsterdam, 1974.
[24] R. Haugsrud, T. Norby, Nature Mater 5 (2006) 193–196.
[25] C.W. Tanner, A.V. Virkar, J. Electrochem. Soc. 143 (1996) 1386–1389.
[26] S.V. Bhide, A.V. Virkar, J. Electrochem. Soc 146 (1999) 2038–2044.
[27] K.H. Ryu, S.M. Haile, Solid State Ionics 125 (1999) 355–367.
[28] K. Katahira, Y. Kohchi, T. Shimura, H. Iwahara, Solid State Ionics 138 (2000) 91–98.
[29] C.D. Savaniu, J. Canales-Vazquez, J.T.S. Irvine, J. Mater. Chem. 15 (2005) 598–604.
[30] N. Zakowsky, S. Williamson, J.T.S. Irvine, Solid State Ionics 176 (2005) 3019–3026.
[31] Z. Zhong, Solid State Ionics 178 (2007) 213–220.
[32] C. Zuo, S.E. Dorris, U. Balachandran, M. Liu, Chem. Mater. 18 (2006) 4647–4650.
[33] H. Matsumoto, Y. Kawasaki, N. Ito, M. Enoki, T. Ishihara, Electrochem. Solid State Lett. 10 (2007) B77–B80.
[34] H.D.A.L. Viana, J.T.S. Irvine, Solid State Ionics 178 (2007) 717–722.
[35] A.K. Azad, J.T.S. Irvine, Solid State Ionics 178 (2007) 635–640.
[36] K. Nomura, K. Tokumistu, T. Hayakawa, Z.J. Homonnay, Radioanalytical and Nuclear Chem 246 (2000) 69–77.
[37] K. Essaki, K. Nakagawa, M. Kato, H.J. Uemoto, Chemical Eng. Japan 37 (2004) 772–777.
[38] K. Nakagawa, T. Ohashi, J. Electrochem. Soc. 145 (1998) 1344–1346.
[39] H.A. Mosqueda, C. Vazquez, P. Bosch, H. Pfeiffer, Chem. Mater. 18 (2006) 2301–2307.
[40] J.C. Abanades, E.S. Rubin, E.J. Anthony, Ind. Eng. Chem. Res. 43 (2004) 3462–3466.
[41] H. Pfeiffer, P. Bosch, Chem. Mater. 17 (2005) 1704–1710.
[42] A. Lopez-Oritz, N.G. Perez-Rivera, A. Reyes Rojas, D.L. Quiterrez, Sep. Sci. Technol. 39 (2004) 3559–3572.
[43] E.O. Fernandez, M. Ronning, T. Grande, D. Chen, Chem. Mater. 18 (2006) 6037–6046.
[44] E.O. Fernandez, M. Ronning, T. Grande, D. Chen, Chem. Mater. 18 (2006) 1383–1385.
[45] B. Feng, W. Liu, X. Li, H. An, Energy and Fuels 20 (2006) 2417–2420.
[46] Y. Li, S. Buchi, J.R. Grace, C.J. Lim, Chem. Mater. 19 (2005) 1927–1934.
[47] T.S. Hang, J. Ma, H.T. Huang, P. Hing, Z.T. Xia, S.H. Chan, J.A. Kilner, Solid State Sciences 5 (2003) 1505–1511.
[48] M. Mogensen, N.M. Sammes, G.A. Tompsett, Solid State Ionics 129 (2000) 63–94.
[49] R.D. Shannon, Acta Crystallogr. A 32 (1976) 751–767.
[50] A.R. West, Basic Solid State Inorganic Chemistry, 2nd Edition, Wiley, New York, 1999;
C.N.R. Rao, J. Gopalakrishnan, New Directions in Solid State Chemistry, 2nd Edition, Cambridge University Press, Cambridge, 1997.
[51] R.H. Mitchell, Perovskites Modern and Ancient, Almaz Press Inc, Ontario, 2002.
[52] M. Vijayakumar, Y. Inaguma, W. Mashiko, M.P.C. Lopez, C. Bohnke, Chem. Mater. 16 (2004) 2719–2724.
[53] W. Huang, P. Shuk, M. Greenblatt, Chem. Mater. 9 (1997) 2240–2245.
[54] J.G. Li, T. Ikegami, T. Mori, T. Wada, Chem. Mater. 13 (2001) 2913–2920.
[55] A.S. Deshpande, N. Pinna, P. Beato, M. Antonietti, M. Niederberger, Chem. Mater. 16 (2004) 2599–2604.
[56] F. Ye, T. Mori, D.R. Ou, J. Zou, J. Drennan, Mater. Res. Bulletin 42 (2007) 943–949.
[57] V. Thangadurai, P. Kopp, J Power Sources 168 (2007) 178–183.
[58] K.R. Priolkar, P. Bera, P.R. Sarode, M.S. Hedge, S. Emura, R. Kumashir, N.P. Lalla, Chem. Mater 14 (2002) 2120–2128.
[59] C. Ho, J.C. Yu, T. Kwong, A.C. Mak, S. Li, Chem. Mater. 17 (2005) 4514–4522.
[60] B. Huang, X.F. Ye, S.R. Wang, H.W. Nie, J. Shi, Q. Hu, J.Q. Qian, X. Sun, T.L. Wen, J. Power Sources 162 (2006) 1172–1181.
[61] C.L. Robert, J.W. Long, E.M. Lucas, K.A. Pettigrew, R.M. Strong, M.S. Doescher, D.R. Rolison, Chem. Mater. 18 (2006) 50–58.
[62] J.T.S. Irvine, D.C. Sinclair, A.R. West, Adv. Mater. 2 (1990) 132–138.
[63] D.Y. Wang, D.S. Park, J. Griffith, A.S. Nowick, Solid State Ionics 2 (1981) 95–105.
[64] G.B. Balazs, R.S. Glass, Solid State Ionics 76 (1995) 155–162.
[65] K. Huang, M. Feng, J.B. Goodenough, J. Am. Ceram. Soc. 81 (1998) 357–362.
[66] C. Tian, S.W. Chan, Solid State Ionics 134 (2000) 89–102.
[67] H. Arai, T. Kunisaki, Y. Shimizu, T. Seiyama, Solid State Ionics 20 (1986) 241–248.
[68] P. Sarkar, P.S. Nicholson, Solid State Ionics 21 (1986) 49–53.
[69] J. Faber, C. Geoffroy, A. Roux, A. Sylvestre, P. Abelard, Appl. Phys. A 49 (1989) 225–232.
[70] Y.J. Park, H. Yoon, E.D. Wachsman, J. Am. Cerm. Soc. 88 (2005) 2402–2408.
[71] B.C.H. Steele, Solid State Ionics 129 (2000) 95–100.
[72] B.C.H. Steele, Solid State Ionics 134 (2000) 3–20.
[73] H. Inaba, H. Tagawa, Solid State Ionics 83 (1996) 1–16.